Title
Single-shot interferometric measurement of cavitation bubble dynamics.

Journal
Optics letters, 46(6)

ISSN
0146-9592

Authors
Wilson, Bryce G
Fan, Zhenkun
Sreedasyam, Rahul
et al.

Publication Date
2021-03-01

DOI
10.1364/ol.416923

Peer reviewed

HHS Public Access

Author manuscript

Opt Lett. Author manuscript; available in PMC 2022 June 26.

Published in final edited form as:

Opt Lett. 2021 March 15; 46(6): 1409–1412. doi:10.1364/OL.416923.

Single shot interferometric measurement of cavitation bubble dynamics

BRYCE G. WILSON[1],

ZHENKUN FAN[1],

RAHUL SREEDASYAM[2],

ELLIOT BOTVINICK[2,3],

VASAN VENUGOPALAN[1,2,3,*]

[1]Department of Chemical and Biomolecular Engineering, University of California, Irvine, CA 92697-2580

[2]Department of Biomedical Engineering University of California, Irvine, CA 92697-2715

[3]Beckman Laser Institute and Medical Clinic, 1002 Health Sciences Rd E, University of California, Irvine, CA 92697-3010

Abstract

We demonstrate an interferometric method to provide direct, single shot measurements of cavitation bubble dynamics with nanoscale spatial and temporal resolution with results that closely match theoretical predictions. Implementation of this method reduces the need for expensive and complex ultra-high speed camera systems for the measurement of single cavitation events. This method can capture dynamics over large time intervals with sub-nanosecond temporal resolution and spatial precision surpassing the optical diffraction limit. We expect this method to have broad utility for examination of cavitation bubble dynamics as well as for metrology applications such as optorheological materials characterization. This method provides an accurate approach for precise measurement of cavitation bubble dynamics suitable for metrology applications such as optorheological materials characterization.

Precise measurement of cavitation dynamics is relevant to phenomena as diverse as sonoluminescence, sonochemistry, molecular transport, fluidic mixing, and light-tissue interactions [1–4]. These phenomena have been exploited in numerous applications including ultrasonic cleaning [6], microfluidic mixing [7] and pumping [8], tissue ablation [5], drug delivery [9,10], ocular surgery [11], microrheology [12,13], screening of cellular mechanosignaling [14,15], and measurement of mechanical properties of soft materials [13,16,17].

Empirical studies providing detailed measurement of cavitation bubble dynamics most often utilize high-speed photographic methods [18,19]. Such measurements are critical

*Corresponding author: vvenugop@uci.edu.

Disclosures. The authors declare no conflicts of interest

to understand complex fluidic processes, assess computational fluid dynamics models, and optimize applications that utilize cavitation bubbles [20]. While the capabilities of high-speed photographic and holographic methods have advanced formidably in recent years, with systems capable of imaging rates as large as 1 trillion frames/second [21–23], significant limitations remain including the total number of frames available, diffraction-limited spatial resolution, and significant expense and complexity. These limitations place these high-speed photography and holography out of the reach of most researchers in terms of cost and/or needed expertise.

On the other hand, time-resolved photography, achieved through combining individual time-gated images from independent cavitation events, has been used by a larger number of investigators [7,24–28]. This approach has enabled the reconstruction of complex bubble dynamics over long-time intervals with high temporal resolution. However, this approach provides an “average” view of the phenomena since the data acquisition utilizes images from different events. This effectively blinds the investigator to important factors that may cause shot-to-shot variability such as the stochastic nature of laser-induced plasma formation and the potential effects of medium heterogeneity and/or impurities [29,30].

As an alternative, investigators have developed optical techniques utilizing probe deflection or spatial transmittance modulation to determine cavitation bubble dynamics [31–34]. However, these techniques appear best suited to probe millimeter scale sized bubbles and generally lack the precision necessary to allow for detailed analysis. Moreover, to obtain quantitative bubble dynamics, these techniques require calibration and/or pairing with photography.

In this Letter, we present a new method for precise measurement of cavitation bubble dynamics with nanoscale temporal resolution and spatial precision. This method utilizes a heterodyne interferometer in a modified Mach-Zehnder configuration [35,36] as shown in Figure 1. To demonstrate its capabilities, we formed cavitation bubbles were formed via laser-induced plasma generation by irradiation using a single 500ps duration pulse emitted by a frequency-doubled Nd:YAG laser (λ=532 nm, Teem Photonics PNG-M03012) laser. The laser beam output was expanded and delivered to a water-filled cuvette using a 40× 0.8 numerical aperture water immersion microscope objective (OBJ, Leica HCX APO L 40x/0.80 W U-V-I). The interferometer was constructed utilizing a polarized continuous wave Helium-Neon laser (HeNe, λ=632.8 nm, 12mW, Newport Optics, R-30993). The separate arms of the interferometer are formed using a 110 MHz acousto-optic modulator (AOM, IntraAction Inc., ATM-1101A1) such that the first-order frequency-shifted beam from the AOM serves as the reference arm and the unshifted beam serves as the sample arm. The sample arm is directed through the cuvette perpendicular to and passing through the center of the bubble. The two beams are recombined using a non-polarizing 50/50 beam splitting cube (BSC, Thorlabs BS013). Dual balanced detection [37] is performed using two 1 GHz bandwidth Si PIN photodiodes (P1 & P2, S5973 Hamamatsu) with the detection circuit enclosed in a steel Faraday cage to reduce ambient electrical noise. The photodiode output signals are amplified using a broadband low-noise amplifier (AMP, Mini-Circuits, ZFL-500LN), digitized by a 2 GHz bandwidth oscilloscope (OSC, LeCroy WaveRunner

6200A) at a sampling rate of 5GS/s, and processed using MATLAB's Hilbert transform function.

Prior to bubble formation the detected interferometer signal consists of a sinusoidal oscillation at the 110 MHz modulation frequency. Bubble formation changes the optical path length of the sample arm as it passes through the growing and collapsing cavity. This dynamic change in optical path length is detected by the photodiodes and prototypical waveforms of both the AOM reference and detected interferometer signals are shown in Figure 2.

The phase difference between the reference and sample arms is directly proportional to the cavitation bubble size. Figure 3 illustrates the results of the Hilbert transform in which both the phase of AOM signal, which is equivalent to the phase of the interferometer reference beam, φref, and phase of the detected interferometer signal, $\varphi sample$, are plotted vs time. The phase difference between these two signals is shown by φbub. Prior to applying the Hibert transform, the raw interferometer signal is processed using notch filters to exclude 314MHz and 629 MHz frequency peaks that correspond to the mode hopping frequency of our HeNe laser. Additionally, a band pass filter between 2.9MHz to 220MHz is used to filter out electrical noise above and below relevant frequency range of the system.

The time-resolved bubble radius $R_B(t)$ is obtained from the optical phase $\varphi_{bub}(t)$ corresponding to the dynamic optical path length difference between the reference and sample arms introduced by the bubble. This leads to the following relationship between the time-resolved bubble radius $R_B(t)$ and the optical phase introduced by the bubble $\varphi_{bub}(t)$

$$R_B(t) = \frac{\lambda \varphi_{bub}(t)}{4\pi(n_G - n_W)} \tag{1}$$

where λ is the wavelength of the probe beam and n_G and n_W are the refractive index of the gas within the bubble and surrounding water, respectively.

Once the bubble is initiated and growing in size, the instantaneous frequency of the interferometer signal I_{int} falls below the 110 MHz heterodyne frequency since the optical Pathlength in the sample arm is decreasing with time. Conversely, once the bubble reaches its maximum size and begins to collapse the instantaneous frequency of the interferometer signal I_{int} rises above 110 MHz heterodyne signal. The detection limit of our bubble measurement is dependent on the phase noise associated with the baseline signal which is 0.1 radians corresponding to 15nm.

To assess the measurement accuracy of the interferometer, we compare the bubble dynamics measurements with predictions provided by the Rayleigh-Plesset model [38] which has been demonstrated to provide accurate predictions for the cavitation bubbl dynamics in this case [13,26]:

$$\rho\left[R_B\frac{d^2R_B}{dt^2} + \frac{3}{2}\left(\frac{dR_B}{dt}\right)^2\right] = p_b - p_\infty - \frac{2\sigma}{R_B} - \frac{4\mu}{R_B}\frac{dR_B}{dt}, \tag{2}$$

where $R_B(t)$ represents the time-resolved bubble radius, μ the viscosity of water, ρ the density of water, and σ the surface tension at water/vapor interface, with p_B and p_∞ representing the pressure inside the bubble and surrounding liquid, respectively. Figure 4 shows excellent agreement between the predictions made by the Rayleigh-Plesset model and the interferometric measurement. As a point of comparison, we also provide bubble dynamics data obtained under similar conditions obtained by taking a single bubble image at different time points using time-resolved photography.

Comparison of the two data sets clearly illustrates the increased measurement uncertainty that is incurred when determining the bubble dynamics using time-resolved images obtained using multiple independent trials. However, we do find that our current interferometric method has difficulty unwrapping the phase during the final stages of bubble collapse once the velocity of the bubble wall exceeds approximately 84–94 m/s. This collapse velocity corresponds to a heterodyne detection frequency in excess of 154–159MHz. Interestingly, we have an unidentified source of ambient electronic noise located at 156 MHz. This leads us to believe that our difficulty in resolving the bubble collapse is not intrinsic to our overall approach but may instead be resolved through better electrical isolation or by using an AOM operating at a lower modulation frequency.

In summary, we have demonstrated an accurate interferometric method for obtaining the complete cavitation bubble dynamics from a single cavitation event with 15nm radial precision and sub-nanosecond temporal resolution. This approach is more accurate, less costly and simpler to operate as compared to fast-frame photographic and holographic methods. Moreover, unlike probe beam methods, our method requires no calibration to obtain quantitative measurements. This approach allows for capturing of the full cavitation bubble dynamics extending over 10's of microseconds while retaining (sub-)nanosecond temporal resolution. We anticipate these capabilities will be of broad utility for examination of cavitation bubble dynamics as well as for metrology applications such as optorheological materials characterization.

Acknowledgements.

BGW acknowledges support of a National Science Foundation (NSF) Graduate Research Fellowship.

Funding.

National Science Foundation (NSF) Graduate Research Fellowship to BGW and National Institutes of Health (R01 GM129426).

FULL REFERENCES

1. Ohl CD, Kurz T, Geisler R, Lindau O, and Lauterborn W, "Bubble dynamics, shock waves and sonoluminescence," Philosophical Transactions of the Royal Society of London. Series A: Mathematical, Physical and Engineering Sciences 357, 269–294 (1999).
2. Didenko YT, McNamara III WB, and Suslick KS, "Effect of noble gases on sonoluminescence temperatures during multibubble cavitation," Physical Review Letters 84, 777 (2000). [PubMed: 11017370]
3. Niemczewski B, "Observations of water cavitation intensity under practical ultrasonic cleaning conditions," Ultrasonics Sonochemistry 14, 13–18 (2007). [PubMed: 16455284]

4. Paliwal S and Mitragotri S, "Ultrasound-induced cavitation: applications in drug and gene delivery," Expert Opinion on Drug Delivery 3, 713–726 (2006). [PubMed: 17076594]
5. Vogel A and Venugopalan V, V, "Mechanisms of pulsed laser ablation of biological tissues," Chemical Reviews 103, 577–644 (2003). [PubMed: 12580643]
6. Yusof NSM, Babgi B, Alghamdi Y, Aksu M, Madhavan J, and Ashokkumar M, "Physical and chemical effects of acoustic cavitation in selected ultrasonic cleaning applications," Ultrasonics Sonochemistry 29, 568–576 (2016). [PubMed: 26142078]
7. Hellman AN AN, Rau KR, Yoon HH, Bae S, Palmer JF, Phillips KS, Allbritton NL, and Venugopalan V, "Laser-induced mixing in microfluidic channels," Analytical Chemistry 79, 4484–4492 (2007). [PubMed: 17508715]
8. Dijkink R and Ohl CD, "Laser-induced cavitation based micropump," Lab on a Chip 8, 1676–1681 (2008). [PubMed: 18813390]
9. Coussios CC and Roy RA, "Applications of acoustics and cavitation to noninvasive therapy and drug delivery," Annual Review of Fluid Mechanics 40, 395–420 (2008).
10. Hellman AN, Rau KR, Yoon HH, and Venugopalan V, "Biophysical response to pulsed laser microbeam-induced cell lysis and molecular delivery," Journal of Biophotonics 1, 24–35 (2008). [PubMed: 19343632]
11. Vogel A, Hentschel W, Holzfuss J, and Lauterborn W, "Cavitation bubble dynamics and acoustic transient generation in ocular surgery with pulsed neodymium: YAG lasers," Ophthalmology 93, 1259–1269 (1986). [PubMed: 3785885]
12. Estrada JB, Barajas C, Henann DL, Johnsen E, and Franck C, "High strain-rate soft material characterization via inertial cavitation," Journal of the Mechanics and Physics of Solids 112, 291–317 (2018).
13. Luo JC, Ching H, Wilson BG, Mohraz A, Botvinick EL, and Venugopalan V, "Laser cavitation rheology for measurement of elastic moduli and failure strain within hydrogels," Scientific Reports 10, 13144 (2020). [PubMed: 32753667]
14. Compton JL, Luo JC, Ma H, Botvinick EL, and Venugopalan V, "High-throughput optical screening of cellular mechanotransduction," Nature Photonics 8, 710–715 (2014). [PubMed: 25309621]
15. Luo JC, Botvinick EL, and Venugopalan V, "Reply to 'Mechanism for microtsunami-induced intercellular mechanosignalling'," Nature Photonics 9, 624–625 (2015).
16. Quinto-Su PA, Kuss C, Preiser PR, and C-D. Ohl, "Red blood cell rheology using single controlled laser-induced cavitation bubbles," Lab on a Chip 11, 672–678 (2011). [PubMed: 21183972]
17. Barney CW, Dougan CE, McLeod KR, Kazemi-Moridani A, Zheng Y, Ye Z, Tiwari S, Sacligil I, Riggleman RA, Cai S S, Lee J-H, Peyton SR, Tew GN, and Crosby AJ, "Cavitation in soft matter," Proceedings of the National Academy of Sciences 117, 9157–9165 (2020).
18. Lauterborn W and Hentschel W, "Cavitation bubble dynamics studied by high speed photography and holography: part one," Ultrasonics 23, 260–8 (1985).
19. Lauterborn W and Hentschel W, "Cavitation bubble dynamics studied by high speed photography and holography: part two," Ultrasonics 24, 59–65 (1986).
20. Lauterborn W, Kurz T, Mettin R, and Ohl C-D, "Experimental and theoretical bubble dynamics," Advances in Chemical Physics 110, 295–380 (1999).
21. Ohl C-D, Philipp A, and Lauterborn W, "Cavitation bubble collapse studied at 20 million frames per second," Annalen der Physik 507, 26–34 (1995)
22. Lauterborn W and Kurz T T, "The bubble challenge for high-speed photography," In The Micro-World Observed by Ultra High-Speed Cameras, Tsuji K, ed. (Springer, 2018), pp. 19–47.
23. Kim T, Liang J, Zhu L, and Wang LV, "Picosecond-resolution phase-sensitive imaging of transparent objects in a single shot," Science Advances 6, eaa6200 (2020).
24. Vogel A, Busch S, and Parlitz U, "Shock wave emission and cavitation bubble generation by picosecond and nanosecond optical breakdown in water," The Journal of the Acoustical Society of America 100, 148–165 (1996).
25. Rau KR, Guerra A, Vogel A, and Venugopalan V, "Investigation of laser-induced cell lysis using time-resolved imaging," Applied Physics Letters 84, 2940–2942 (2004).

26. Rau KR, Quinto-Su PA, Hellman AN, and Venugopalan V, "Pulsed laser microbeam-induced cell lysis: time-resolved imaging and analysis of hydrodynamic effects," Biophysical Journal 91, 317–329 (2006). [PubMed: 16617076]
27. Quinto-Su PA, Lai HH, Yoon HH, Sims CE, Allbritton NL, and Venugopalan V, "Examination of laser microbeam cell lysis in a PDMS microfluidic channel using time-resolved imaging," Lab on a Chip 8, 408–414 (2008). [PubMed: 18305858]
28. Compton JL, Hellman AN, and Venugopalan V, "Hydrodynamic determinants of cell necrosis and molecular delivery produced by pulsed laser microbeam irradiation of adherent cells," Biophysical Journal 105, 2221–2231 (2013). [PubMed: 24209868]
29. Linz N, Freidank S, Liang XX, Vogelmann H, Trickl T, and Vogel A, "Wavelength dependence of nanosecond infrared laser-induced breakdown in water: Evidence for multiphoton initiation via an intermediate state," Physical Review B 91, 134114 (2015).
30. Tian Y, Xue B, Song J, Lu Y, and Zheng R, "Stabilization of laser-induced plasma in bulk water using large focusing angle," Applied Physics Letters, 109, 061104 (2016).
31. Gregorčič P and Možina J, "A beam-deflection probe as a method for optodynamic measurements of cavitation bubble oscillations," Measurement Science and Technology, 18, 2972 (2007).
32. Gregorčič P, Možina J, and Močnik G, "Measurements of cavitation bubble dynamics based on a beam-deflection probe," Applied Physics A 93, 901–905 (2008).
33. Petkovšek R and Gregorčič P, "A laser probe measurement of cavitation bubble dynamics improved by shock wave detection and compared to shadow photography," Journal of Applied Physics, 102, 044909 (2007).
34. Devia-Cruz LF, Camacho-López S, Cortés VR, Ramos-Muñiz V, Pérez-Gutiérrez FG, and Aguilar G, "Reconstruction of laser-induced cavitation bubble dynamics based on a Fresnel propagation approach," Applied Optics 54, 10432–10437 (2015). [PubMed: 26836867]
35. Yablon AD, Nishioka NS, Mikić BB, and Venugopalan V, "Measurement of tissue absorption coefficients by use of interferometric photothermal spectroscopy," Applied Optics 38, 1259–1272 (1999) [PubMed: 18305741]
36. Carp SA, Guerra III A, Duque SQ Jr, and Venugopalan V, "Optoacoustic imaging using interferometric measurement of surface displacement," Applied Physics Letters, 85, 5772–5774 (2004).
37. Abbas G, Chan V, and Yee T, "A dual-detector optical heterodyne receiver for local oscillator noise suppression," Journal of Lightwave Technology 3, 1110–1122 (1985).
38. Brennan CE, Cavitation and Bubble Dynamics (Oxford University Press, 1995).

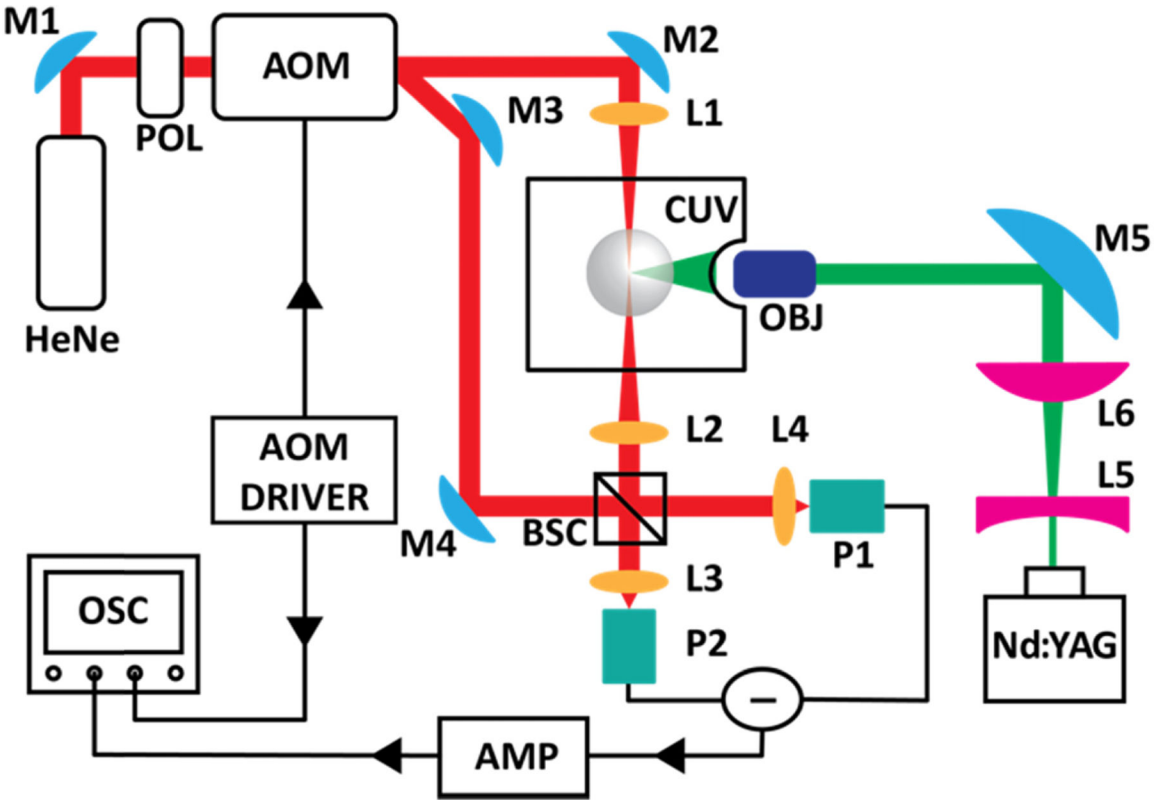

Fig. 1:

Diagram of the Mach-Zehnder interferometric system. M1-M5 are 1 inch silver mirrors used to direct both the pump (Nd:YAG) and interferometer probe (HeNe) beams. 50mm convex lenses L1 & L2 are used to direct the interferometer probe beam through the bubble. 10mm convex lenses L3 & L4 are used to focus the combined interferometer beams onto the Si-PIN diodes P1 and P2. 50mm concave (L5) and 125 mm convex (L6) lenses are used to expand and recollimate the Nd:YAG pump beam.

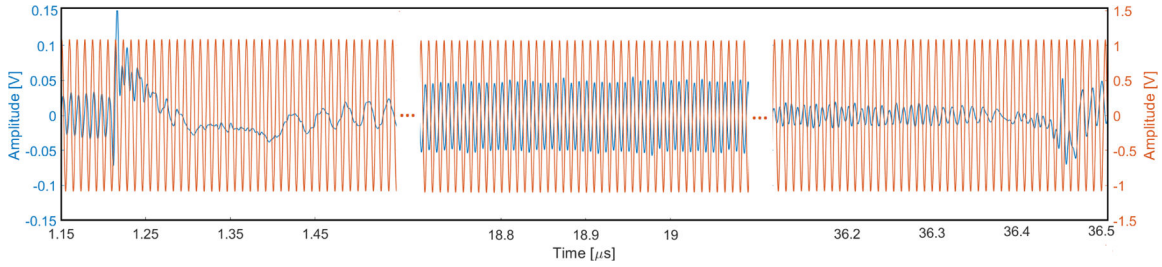

Fig. 2:

Recovered Photodiode signal and AOM driving signal from oscilloscope following initiation of a cavitation bubble using a 20μJ. I_{int} (blue) and I_{aom} (orange) are shown in segments corresponding to (a) the beginning, (b) middle and (c) end of bubble a 175μm diameter bubble created by a 20uJ laser pulse.

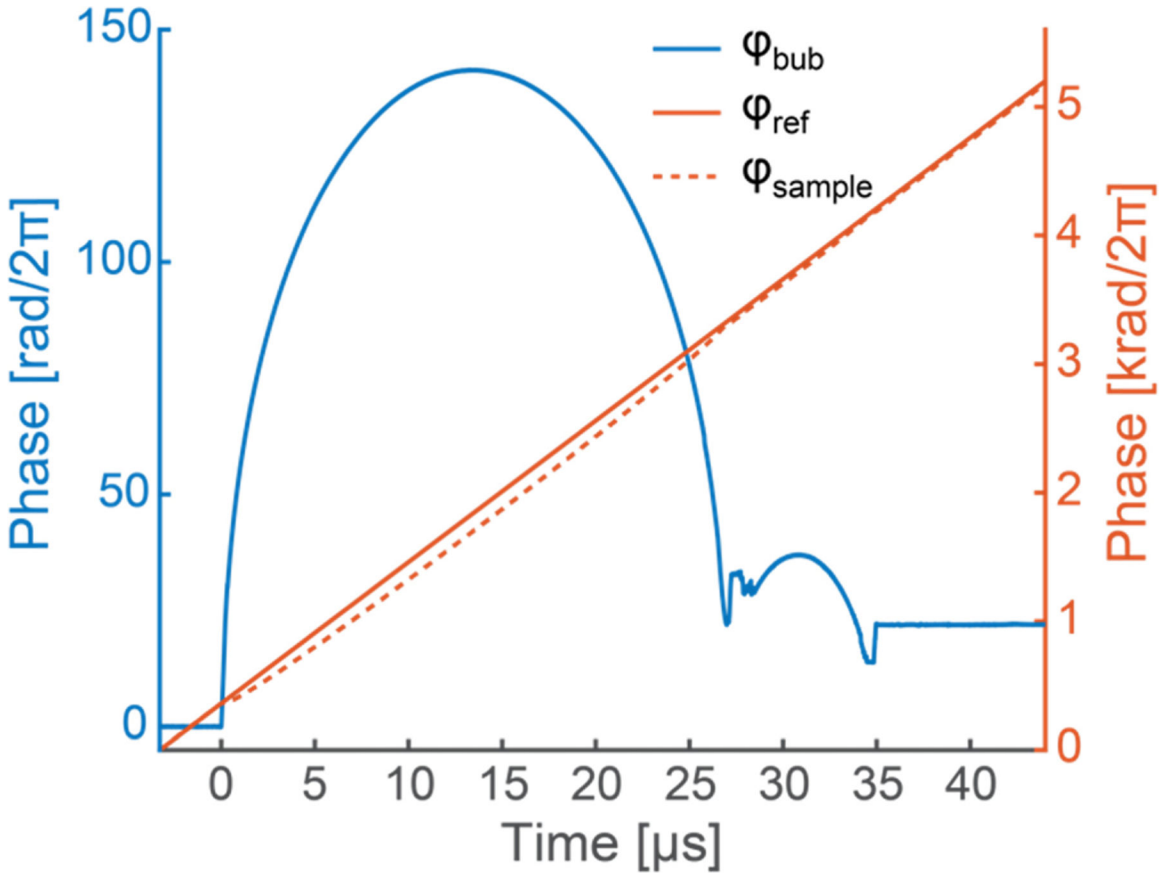

Fig. 3:

Measured φref and φint corresponding to the formation of a 141.3 μm diameter cavitation bubble using a 10μJ laser pulse. φbub is the phase difference between the reference and interferometer signals.

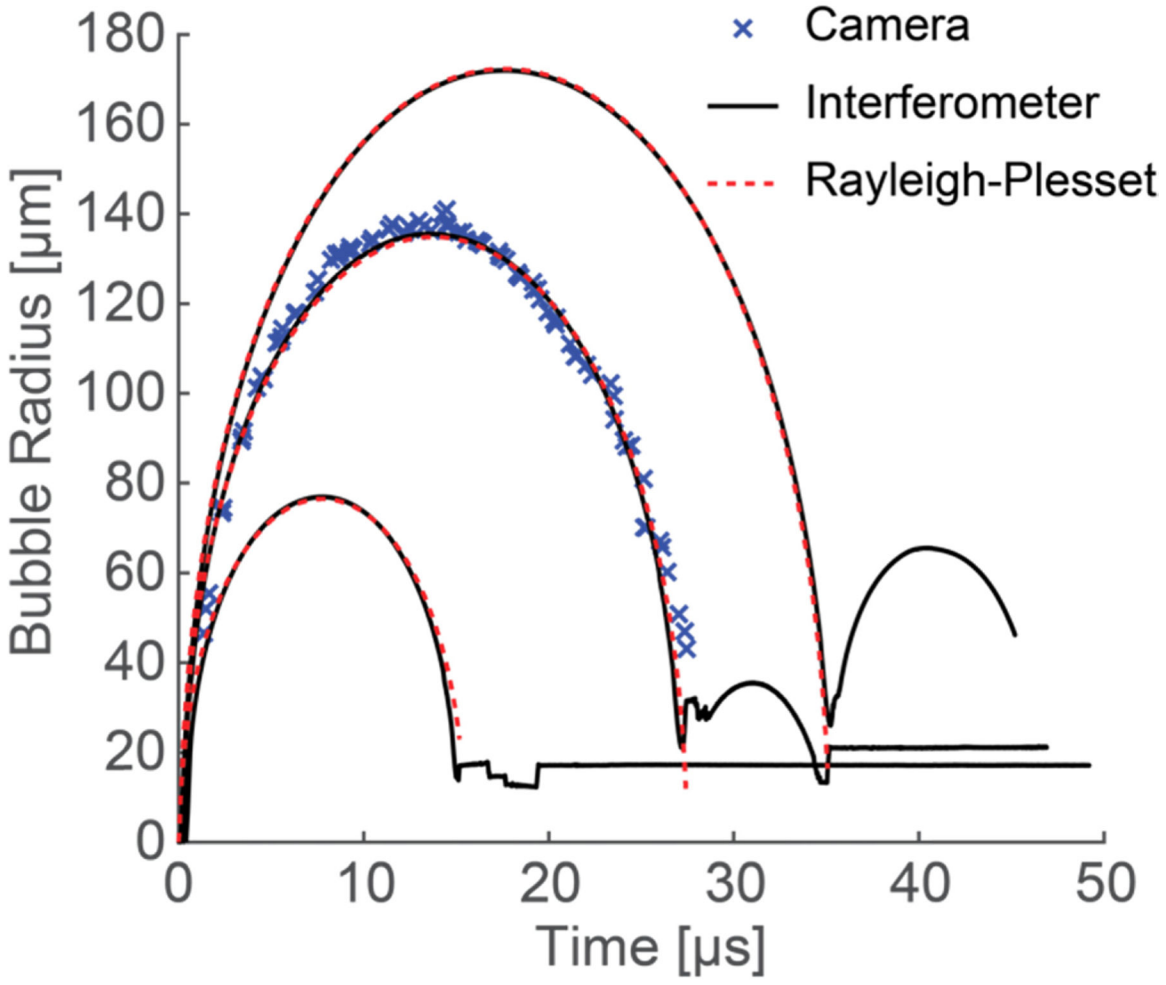

Fig. 4:

Time resolved bubble dynamics for bubbles formed using pulse energies of 2.5, 10, and 20 μJ resulting in maximum bubble radii of 77, 136, and 172 μm, respectively, is shown with theoretical bubble radius predicted by the Rayleigh-Plesset model. In the case of the 10μJ pulse energy, we also show data acquired using images from captured from separate events using an intensified CCD camera.